Contrib Mineral Petrol (2009) 158:471–484
DOI 10.1007/s00410-009-0392-7

ORIGINAL PAPER

# Water diffusion in Mount Changbai peralkaline rhyolitic melt

**Haoyue Wang · Zhengjiu Xu · Harald Behrens · Youxue Zhang**

Received: 30 October 2008 / Accepted: 20 February 2009 / Published online: 12 March 2009


**Abstract** Diffusion couple experiments with wet half (up to 4.6 wt%) and dry half were carried out at 789–1,516 K and 0.47–1.42 GPa to investigate water diffusion in a peralkaline rhyolitic melt with major oxide concentrations matching Mount Changbai rhyolite. Combining data from this work and a related study, total water diffusivity in peralkaline rhyolitic melt can be expressed as:

$$D_{H_2O_t} = D_{H_2O_m}\left(1 - \frac{0.5 - X}{\sqrt{[4\exp(3110/T - 1.876) - 1](X - X^2) + 0.25}}\right),$$

with $D_{H_2O_m} = \exp\left[-12.789 - \frac{13939}{T} - 1229.6\frac{P}{T} + (-27.867 + \frac{60559}{T})X\right]$,

where $D$ is in $m^2\ s^{-1}$, $T$ is the temperature in K, $P$ is the pressure in GPa, and $X$ is the mole fraction of water and calculated as $X = (C/18.015)/(C/18.015 + (100 - C)/33.14)$, where $C$ is water content in wt%. We recommend this equation in modeling bubble growth and volcanic eruption dynamics in peralkaline rhyolitic eruptions, such as the ~1,000-AD eruption of Mount Changbai in North East China. Water diffusivities in peralkaline and metaluminous rhyolitic melts are comparable within a factor of 2, in contrast with the 1.0–2.6 orders of magnitude difference in viscosities. The decoupling of diffusivity of neutral molecular species from melt viscosity, i.e., the deviation from the inversely proportional relationship predicted by the Stokes–Einstein equation, might be attributed to the small size of $H_2O$ molecules. With distinct viscosities but similar diffusivity, bubble growth controlled by diffusion in peralkaline and metaluminous rhyolitic melts follows similar parabolic curves. However, at low confining pressure or low water content, viscosity plays a larger role and bubble growth rate in peralkaline rhyolitic melt is much faster than that in metaluminous rhyolite.

**Keywords** $H_2O$ diffusion · Peralkaline rhyolite · Stokes–Einstein equation · Bubble growth

## Introduction

Water diffusion data in natural melts are crucial to the understanding and quantitative modeling of bubble growth in a magma chamber or during magma ascent (e.g., Proussevitch and Sahagian 1998; Liu and Zhang 2000), magma degassing (e.g., Self et al. 2008), and magma fragmentation in explosive volcanic eruption (e.g., Zhang 1999a; Spieler et al. 2004; Zhang et al. 2007). As the major volatile in silicate melts, water strongly affects their physical properties (density and viscosity, e.g., Shaw 1972; Ochs and Lange 1999; Zhang et al. 2003); and hence $H_2O$ diffusion in magma may also alter the dynamics of magma transport (Melnik and Sparks 1999; Blower et al. 2001).

Communicated by T. L. Grove.

H. Wang · Y. Zhang
MOE Key Laboratory of Orogenic Belts, School of Earth and Space Sciences, Peking University, 100871 Beijing, China

H. Wang · Z. Xu · Y. Zhang (✉)
Department of Geological Sciences, The University of Michigan, Ann Arbor, MI 48109-1005, USA
e-mail: youxue@umich.edu

H. Behrens
Institute für Mineralogie, Universität Hannover, Callinstr. 3, 30167 Hannover, Germany

To extract diffusivities, $H_2O$ diffusion experiments have been carried out in various melts, ranging from rhyolite (e.g., Shaw 1974; Delaney and Karsten 1981; Zhang et al. 1991; Nowak and Behrens 1997; Zhang and Behrens 2000; Ni and Zhang 2008) to dacite and andesite (Liu et al. 2004; Behrens et al. 2004; Okumura and Nakashima 2006; Ni et al. 2009a, b) to depolymerized basalt (Zhang and Stolper 1991; Okumura and Nakashima 2006). $H_2O$ diffusion in "normal" metaluminous or calc-alkaline rhyolitic melt (metaluminous and calc-alkaline will be used interchangeably) is the most extensively studied in terms of temperature, pressure and $H_2O$ concentration coverage. The work on other melts is limited.

Mount Changbai Volcano at the border between China and North Korea has produced explosive peralkaline rhyolitic eruptions, including a $\sim$30-km$^3$ eruption at about 1,000 AD (Jin and Zhang 1994; Horn and Schmincke 2000). The peralkaline rhyolite melt is less viscous than the "normal" metaluminous rhyolite investigated for $H_2O$ diffusion by previous authors by 1.0–2.6 orders of magnitude (Table 1; see more discussion of viscosity models later). The lower viscosity of peralkaline rhyolite can be attributed to extra alkali ions not associated with aluminum ions, thus a decrease in the degree of polymerization. The Stokes–Einstein relation (Einstein 1905) implies that the diffusivity of large neutral molecular species is inversely proportional to viscosity. Even though the Stokes–Einstein relation has been shown to be inapplicable to $H_2O$ diffusion in silicate melts (e.g., Ni and Zhang 2008), there may still be a significant increase of $H_2O$ diffusivity from metaluminous rhyolitic melt to peralkaline rhyolitic melt. Furthermore, it was found that $H_2O$ diffusivity in sodium tetrasilicate glass (Scholze and Mulfinger 1959) is three orders of magnitude faster than that in silica glass (Moulson and Roberts 1961). Hence, $H_2O$ diffusion may be significantly faster in peralkaline rhyolite than in metaluminous rhyolite, and this would lead to much higher bubble growth rates as well as different eruption dynamics. To quantify the compositional effect, two experimental studies on $H_2O$ diffusion in peralkaline rhyolite have been conducted, one on peralkaline and peraluminous samples with total $H_2O$ content $\leq$2.3 wt% (Behrens and Zhang 2009), and this report on $H_2O$ diffusion in Mount Changbai peralkaline rhyolitic melt to total $H_2O$ content of 4.6 wt%. Another purpose of this work is to provide the basic data for specific modeling of bubble growth and volcanic eruption dynamics in past and future Mount Changbai eruptions and other eruptions of similar peralkaline rhyolites.

**Table 1** The anhydrous composition (wt%) of Changbai peralkaline rhyolite, synthesized peralkaline rhyolite (CB) in this study, NSL glass, and a metaluminous rhyolite

| | Changbai rhyolite[a] | CB[b] | NSL[a] | Metaluminous rhyolite[c] |
|---|---|---|---|---|
| $SiO_2$ | 75.74 | 76.38 | 75.45 | 76.87 |
| $TiO_2$ | 0.22 | 0.2 | 0.19 | 0.04 |
| $Al_2O_3$ | 10.11 | 10.32 | 10.05 | 13.38 |
| $FeO_T$ | 4.00 | 4.37 | 4.29 | 0.97 |
| MnO | 0.08 | 0 | 0.12 | 0.04 |
| MgO | 0.02 | 0 | 0.00 | 0.03 |
| CaO | 0.22 | 0 | 0.17 | 0.55 |
| $Na_2O$ | 4.57 | 5.11 | 5.27 | 4.14 |
| $K_2O$ | 4.36 | 4.66 | 4.56 | 4.65 |
| $P_2O_5$ | 0.03 | 0 | 0 | 0.01 |
| Total | 99.35 | 101.04 | 100.1 | 100.68 |
| Viscosity[d] (Pa s) of dry melt at 1,123 K | – | $10^{8.28}$ | $10^{8.10}$ | $10^{10.93}$ |
| Viscosity[d] (Pa s) of hydrous melt (with 4.0 wt% $H_2O$) at 1,123 K | – | $10^{3.66}$ | $10^{3.62}$ | $10^{4.67}$ |

[a] Data from Horn and Schmincke (2000) and Behrens and Zhang (2009)

[b] Measured by SX100 electron probe microanalyser in the University of Michigan, with acceleration voltage of 15 Kev, beam current of 1 nA, and beam size of 10 μm

[c] Rhy4 in Ni and Zhang (2008) was chosen to represent the metaluminous rhyolite

[d] Calculated from the viscosity model of Hui and Zhang (2007)

## Experimental and analytical methods

### Starting materials

Phenocryst-free and bubble-free glass is not available from Mount Changbai eruption products. Hence, the starting materials (both dry and hydrous peralkaline glasses) are synthesized. Anhydrous peralkaline rhyolitic glass with a composition similar to Changbai rhyolite was prepared by fusing oxides and carbonates at 1,873 K in air (Ohlhorst et al. 2001). This glass is named CB. To obtain large pieces of homogeneous hydrous glass (0.6–0.8 g), powder of anhydrous glass and water were loaded into an $Au_{80}Pd_{20}$ capsule (6 mm in diameter and 30 mm in length) in turn in several portions. Syntheses of samples with 1.3–6.2 wt% $H_2O_t$ were performed in an internally heated pressure vessel (IHPV) at 1,473–1,523 K and 0.3–0.5 GPa for 13–48 h at University of Hannover. Accumulation of stress in the glasses after cooling was a major problem for the preparation of large pieces of Changbai peralkaline rhyolite. Syntheses finished with a standard initial cooling rate of 200 K min$^{-1}$ often yielded fragmented glasses. To minimize stress in the glasses we adopted the following cooling procedure: 50 K min$^{-1}$ down to 973 K, 10 K min$^{-1}$ from 973–673 K, and 5 K min$^{-1}$ below 673 K. This cooling

procedure was slow enough to enable stress relaxation during cooling and fast enough to avoid crystallization. Pieces of the synthesized glass (usually from glass in contact with the capsule or at the two ends) were polished and checked under optical microscope. No quench crystals or bubbles were found.

The synthesized peralkaline rhyolitic glasses (CB) have been analyzed by electron microprobe at the University of Michigan. Table 1 lists the anhydrous composition of the synthesized glasses CB, and the composition of Changbai peralkaline rhyolite. For comparison, the composition of NSL (another peralkaline rhyolite studied by Behrens and Zhang 2009), and that of the metaluminous rhyolite studied by numerous previous authors (e.g., Shaw 1974; Delaney and Karsten 1981; Zhang et al. 1991; Zhang and Behrens 2000; Ni and Zhang 2008) are also given in Table 1. The viscosities at 1,123 K (a typical rhyolitic eruption temperature) calculated from the model of Hui and Zhang (2007) are also listed (see later discussion on viscosity models). The calculated viscosities of CB and NSL are similar, but are 1.0–2.6 orders of magnitude lower than that of the "normal" metaluminous rhyolite.

## Calibration for the measurement of $H_2O$ in peralkaline rhyolitic glasses by IR

Pieces of the synthesized peralkaline rhyolitic glasses have been measured for the total $H_2O$ content (hereafter denoted as $H_2O_t$) using Karl–Fischer titration (KFT) at University of Hannover, following the procedures of Behrens et al. (1996). The raw data were corrected for unextracted water after analyses by adding 0.10 wt% $H_2O$ (Leschik et al. 2004). The uncertainty of the $H_2O_t$ is about ±0.10 wt%, estimated from the error of the unextracted water (±0.05 wt%) and the error of the titration rate (±0.02 μg $s^{-1}$).

To measure $H_2O$ diffusion profiles using Fourier transform infrared spectroscopy (FTIR), we have calibrated the FTIR method using the KFT results. The set of samples for the calibration contains $H_2O_t$ contents of 1.31, 1.36, 2.14, 3.13, 3.33, 3.96, 4.31, and 6.21 wt% according to KFT measurements.

Infrared (IR) analyses of the glasses have been conducted using a Perkin–Elmer FTIR (Spectrum GX) with a NIR (near infrared) source, $CaF_2$ beamsplitter, and a liquid-$N_2$ cooled InSb detector. The molecular $H_2O$ (hereafter denoted as $H_2O_m$) peak is at wavenumber of 5,230 $cm^{-1}$, and the hydroxyl (hereafter denoted as OH) peak is at wavenumber of 4,520 $cm^{-1}$ in NIR spectra of CB (Stolper 1982; Fig. 1). For simplicity, linear absorbance (instead of integrated absorbance) of each peak is determined. Two different kinds of baselines were tried. One is by drawing a straight line tangential to the background on both sides of the peak (TT method in Withers and Behrens 1999). And

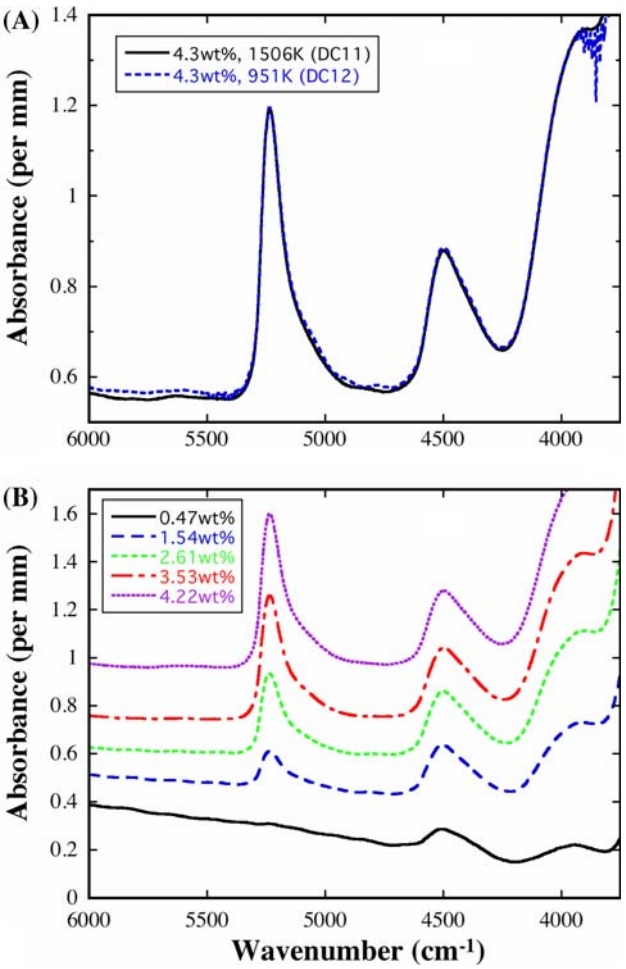


**Fig. 1** **a** IR spectra at the flat high water content region in two experiments with different temperatures. Baseline of DC12 in this figure is shifted for clear comparison. **b** IR spectra from one end to the other in a diffusion profile (DC12), with water content in the legend. Baseline is offset for clarity

the other is by using a flexible curve to fit the background (FC method in Withers and Behrens 1999; Zhang 1999b). The FTIR and KFT data are used to calibrate the molar absorptivities (or extinction coefficients). The general relation between FTIR and KFT data is (Stolper 1982):

$$C = C_1 + C_2 = \frac{18.015A_{523}}{\rho d\varepsilon_{523}} + \frac{18.015A_{452}}{\rho d\varepsilon_{452}}, \quad (1)$$

where $C$ is $H_2O_t$ content (in mass fraction), $C_1$ is $H_2O_m$ content, $C_2$ is the mass fraction of water dissolved in the glass as OH, 18.015 is the molar mass of $H_2O$, $A_{523}$ is the linear absorbance of the 5,230 $cm^{-1}$ peak using transmission FTIR, $A_{452}$ is the linear absorbance of the 4,520 $cm^{-1}$ peak, $\rho$ is the density of the hydrous glass, $d$ is the sample thickness, and $\varepsilon_{523}$ and $\varepsilon_{452}$ are the linear molar absorptivities of the 5,230 and 4,520 $cm^{-1}$ peaks. The density was measured using the buoyancy method by weighing single glass pieces in air and in water. Based on a set of 10 hydrous

samples with water contents ranging from 0.8 to 6.3 wt%, the following density–water content relationship was obtained:

$$\rho = 2415 - 12.5w, \quad (2)$$

where $\rho$ is in kg $m^{-3}$ and the water content $w$ is in wt%. This relationship reproduces the experimental density data within 15 kg $m^{-3}$ except for one outlier. The implied partial molar volume of $H_2O$ in the glass is $(11.4 \pm 0.1) \times 10^{-6}$ $m^3$ $mol^{-1}$, in agreement with $(12.0 \pm 0.5) \times 10^{-6}$ $m^3$ $mol^{-1}$ of Richet et al. (2000).

The molar absorptivities $\varepsilon_{523}$ and $\varepsilon_{452}$ are determined by linear regression after converting Eq. 1 to the following form (Behrens et al. 1996):

$$\frac{18.015A_{523}}{\rho dC} = \varepsilon_{523} - \frac{\varepsilon_{523}}{\varepsilon_{452}} \frac{18.015A_{452}}{\rho dC}. \quad (3)$$

By plotting $18.015\bar{A}_{523}/(\rho C)$ versus $18.015\bar{A}_{452}/(\rho C)$, the $y$-intercept gives $\varepsilon_{523}$, and the slope gives $-\varepsilon_{523}/\varepsilon_{452}$. From the slope and intercept, $\varepsilon_{452}$ (the $x$-intercept) can be calculated. Figure 2 shows the calibration using both straight-line baselines and curved baselines. It turns out that the calibration for this peralkaline rhyolitic glass using curved baselines is not much different from that for the metaluminous rhyolite (Newman et al. 1986). With our limited data, straight-line baselines and curved baselines fittings have about the same reproducibility. Hence, for simplicity, the straight-line baselines with $\varepsilon_{523} = 0.159$ L $mol^{-1}$ $mm^{-1}$ and $\varepsilon_{452} = 0.182$ L $mol^{-1}$ $mm^{-1}$ are adopted hereafter. Although the calibration may not be as accurate as we would like in terms of calculation of species concentrations, the exact determination of the concentration of hydrous species (OH and $H_2O_m$) is not required for the determination of total water diffusivity.

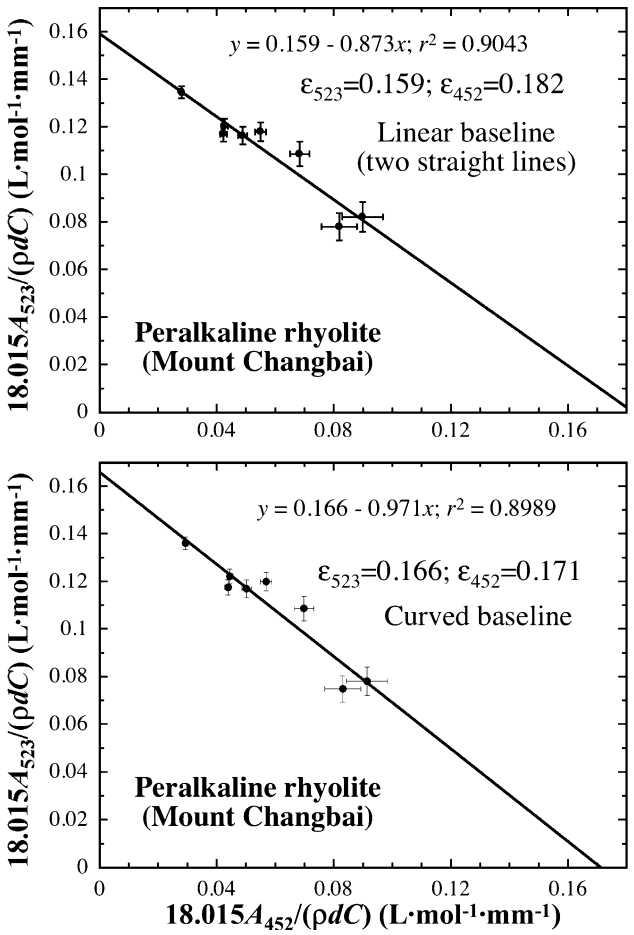


**Fig. 2** Calibration to derive the molar absorptivities for peralkaline rhyolitic glass for straight-line baseline and curved baseline

## Diffusion couple experiments

Diffusion couple experiments were carried out in an end-loaded piston cylinder apparatus at the University of Michigan, generally following the procedures of Ni and Zhang (2008). Each diffusion couple is made of a dry peralkaline rhyolite half and a hydrous peralkaline rhyolite half. Each half is a cylinder with a diameter of about 2.5 mm and a thickness of 1–2 mm. The hydrous half is thicker than the dry half by more than 50% because diffusion in the hydrous half is more rapid. One base of each half is polished.

In an experiment, the dry and hydrous halves are joined together so that they are in contact at the polished surfaces, and placed in a graphite capsule, with the less dense hydrous one on top of the other to mitigate convection (Fig. 3). For experiments at temperatures lower than the melting point of gold, the graphite capsule is emplaced in a gold capsule, followed by squeezing to minimize air and free space in it to reduce internal stress inside the capsule, and welding. Then the capsule with the sample charge is placed in a drilled MgO rod, covered by a thin MgO wafer to separate the thermocouple tip from the graphite or gold capsule. The MgO rod with the capsule is placed in a graphite heater. Then an MgO tube and the thermocouple inside its sleeve are inserted into the graphite furnace. The furnace is further inserted into a $BaCO_3$ cell as the pressure medium, which is wrapped with a lead foil as the lubricant, making up the sample assembly. The lengths of all parts were designed so that the diffusion couple interface was at the hotspot. In the experiment CB-PR-DC5, a gold capsule was used although the experimental temperature was higher than the melting point of gold. Nonetheless, the thermocouple did not fail and the temperature during experiment was stable, probably because the thin MgO wafer between the thermocouple and gold prevented any contacts and contamination of thermocouple by molten gold.

Temperature and pressure were monitored by a Type-D thermocouple ($Re_3W_{97}$-$Re_{25}W_{75}$) and a pressure gauge, respectively. A LabVIEW computer program continuously recorded the temperature, providing the detailed thermal

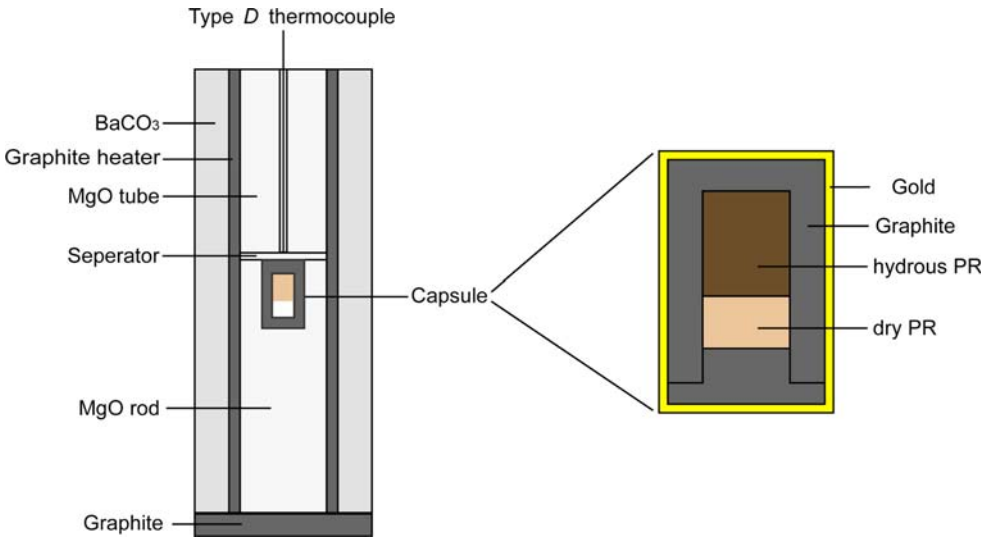


**Fig. 3** A sketch of the experimental assembly with the capsule enlarged at the right hand side. The scale is not exact. PR means peralkaline rhyolite glass. The dry part is thinner than the hydrous part because diffusivity is smaller at lower $H_2O_t$. After Ni et al. (2009a)

history. The temperature at the interface of the diffusion couple (roughly at the center of the graphite heater and assumed to be the hot spot) differs from that recorded by the thermocouple because the thermocouple tip is a couple of millimeters away from the sample. Temperature at the hot spot was calculated by estimating the distance between the thermocouple tip and the diffusion couple interface and applying the calibrated temperature gradient inside the charge (Hui et al. 2008). The temperature correction is typically about 20 K. On the other hand, the temperature variation along the full length of a diffusion couple (about 3-mm long, or ±1.5 mm from the center) is only about 4 K. The difference between 4 and 20 K is because a graphite cap and an MgO wafer further separate the thermocouple tip from the sample. Hui et al. (2008) and Ni and Zhang (2008) conducted pressure calibrations for the two piston–cylinder apparatuses at the University of Michigan, which shows that the real pressure in the piston–cylinders is on average 5.5% lower than the nominal pressure. This correction is applied here.

An experiment was started by bringing the pressure to the desired value using a piston-out procedure. Next the sample charge was heated up to and maintained at about 473 K for the charge to relax for several hours to overnight. Then the temperature was brought up to the intended experimental temperature while manually maintaining the desired pressure. After a planned duration at high temperature, the power to the heater was turned off to quench the sample charge. The initial quench rate is of the order 100 K $s^{-1}$, depending on the initial temperature. Efforts were made to maintain a constant pressure by manual pumping during quench. The experimental duration was designed so that it was long enough to generate a long diffusion profile to mitigate convolution effects (i.e., each measurement gives an average concentration of a finite region due to the limited spatial resolution in infrared analyses but we need the concentration at a given point), yet short enough so that the two ends are unaffected by diffusion and that crystallization is minimized if the experimental temperature is below the liquidus of the melt. The effect of diffusion during heating up and quenching was corrected by calculating an effective experimental duration as in Zhang and Stolper (1991), and the correction is about 10 s, <6% of the experimental duration for the shortest-duration experiment. Seven experiments were successful (Table 2). Several other experiments are deemed unsuccessful due to either thermocouple failure or crystallization. In addition, we made efforts to obtain experimental diffusion data at pressures of 1.0 and 1.5 GPa and below-liquidus temperatures. Unfortunately, these experiments all failed due to crystallization. The increased ease of crystallization as pressure is increased for this composition is consistent with experiments on metaluminous rhyolite (Hui et al. 2008; Ni and Zhang 2008), and may be attributed to greater undercooling and higher melt density at higher pressure.

## Measurement of water concentration profile by infrared analysis

After each experiment, the quenched charge was mounted in epoxy resin and doubly polished to a thin wafer of ~0.2-mm thickness exposing a rectangular section containing the cylindrical axis, along which the diffusion of interest happened. Cracks that are subparallel to the diffusion couple interface are observed in all sections, presumably due to the non-hydrostatic stress during cooling. The presence of cracks causes at least two complexities. One is that every crack means a part of the profile cannot be measured. Secondly, due to shrinkage and possible shifting during polishing, the distance across a crack may not be the real distance. Sometimes subtraction of distance is needed to smooth the concentration profile across a crack.

**Table 2** Summary of experimental conditions and results

| Exp. # | $T$ (K) | $P$ (GPa) | Duration (s) | Thickness (mm) | Final $H_2O_t$ (wt%) | Profile length (mm) |
|---|---|---|---|---|---|---|
| CB-PR-DC1 | 1297 ± 10 | 0.47 | 610 | 0.217 | 4.6/0.07 | 0.531 |
| CB-PR-DC2 | 789 ± 10 | 0.47 | 42,970 | 0.174 | 4.4/0.12 | 0.422 |
| CB-PR-DC3 | 944 ± 10 | 0.47 | 4,084 | 0.204 | 4.6/0.08 | 0.400 |
| CB-PR-DC5 | 1516 ± 15 | 1.42 | 460 | 0.235 | 4.3/0.20 | 0.733 |
| CB-PR-DC11 | 1506 ± 15 | 0.47 | 196 | 0.220 | 4.3/0.24 | 0.553 |
| CB-PR-DC12 | 951 ± 15 | 0.47 | 7,173 | 0.185 | 4.3/0.29 | 0.655 |
| CB-PR-DC13 | 1496 ± 15 | 0.95 | 318 | 0.155 | 4.1/0.14 | 0.500 |

Uncertainty in temperature is given at $2\sigma$ level. Final $H_2O_t$ (wt%): averaged $H_2O_t$ contents at the high and low flat regions of the diffusion profile. The definition of the profile length can be found in the text

The doubly polished wafers were measured for $H_2O_t$ concentration (as well as for species concentrations) by FTIR using the calibration discussed earlier, and the Perkin–Elmer FTIR microscope with an automated stage (a 10-μm wide aperture, NIR source, $CaF_2$ beamsplitter, MCT detector). Spectra were hand-fit with tangential baselines, and the peak heights obtained at 5,230 and 4,500 $cm^{-1}$ were used to calculate $H_2O_m$ and OH concentrations, the sum of which is $H_2O_t$ concentration. At low water concentration, since the peak height at 5,230 $cm^{-1}$ is essentially zero and that at 4,520 $cm^{-1}$ is noisy, in some cases the peak height at 3,570 $cm^{-1}$ was measured. To be consistent, this extinction coefficient was assigned with a value that ensures continuity in $H_2O_t$ concentrations for these cases.

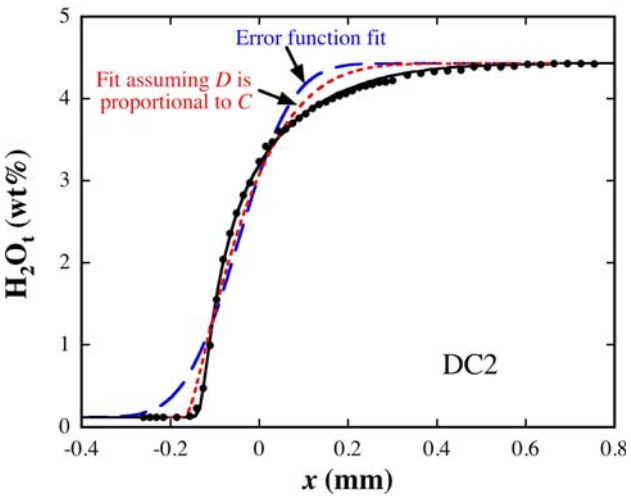


**Fig. 4** $H_2O_t$ diffusion profile in experiment DC2 and various fits to the profile. Data are shown as points. The *blue long-dashed curve* is a fit by the error function. The *red short dashed curve* is a fit by assuming $D_{H_2O_t}$ is proportional to $H_2O_t$ concentration. The *black solid curve* is a fit by assuming (1) $D_{OH} \ll D_{H_2O_m}$ and (2) $D_{H_2O_m} = D_0 e^{aX}$ where $X$ is mole fraction of $H_2O_t$, and $D_0$ and $a$ are two fitting parameters

## Experimental results

Conditions of seven successful experiments are listed in Table 2, and their corresponding $H_2O_t$ concentration profiles are shown in Figs. 4 and 5. Only the part of the profile affected by diffusion within the couple is displayed in the figures. For one experiment (DC12), successive IR spectra at different locations are shown (Fig. 1b). Because the equilibrium of $H_2O_m$ and OH at high temperature cannot be preserved during quenching, their concentrations are not shown here and are not directly used in obtaining diffusivity (Zhang et al. 1995, 1997b; Behrens and Nowak 2003). This can be seen in Fig. 1a that at the same water content, IR spectra are essentially the same for both 1,506 and 951 K experiments, indicating the measured speciation in quenched sample was that at an apparent equilibrium temperature related to quenching rate rather than experimental temperature.

Convolution tends to prolong and distort the real diffusion profile. To address this issue, we compare the length of each diffusion profile with the spatial resolution of IR beam. First, we define a diffusion length for each profile as the distance between the two points with the concentration of $C_{Lo} + 0.05(C_{Hi} - C_{Lo})$ and $C_{Lo} + 0.95(C_{Hi} - C_{Lo})$, where $C_{Lo}$ and $C_{Hi}$ are the average $H_2O_t$ at dry and hydrous ends. The asymptotic behavior at one end of each diffusion profile makes the above arbitrary definition necessary. The profile lengths are listed in Table 2. As discussed by Ni et al. (2009a), if the aperture width is 10 μm, the divergence of the beam inside the glass sample results in a full width at half maximum (FWHM) of about 15 μm. Because the length of every profile is more than 26 times FWHM, far greater than the critical 8 times FWHM suggested by Ganguly et al. (1988), the convolution effects are expected to be insignificant in the determination of diffusivity.

All $H_2O_t$ diffusion profiles shown in Figs. 4 and 5 differ from an error function shape (Fig. 4 shows that the profile cannot be fitted well by an error function) and lack a center of symmetry, indicating that the diffusion coefficient of $H_2O_t$ is not a constant but is dependent on $H_2O_t$ concentration. This characteristic has been observed repeatedly for $H_2O_t$ diffusion profiles in rhyolitic, dacitic and basaltic melts (e.g.,

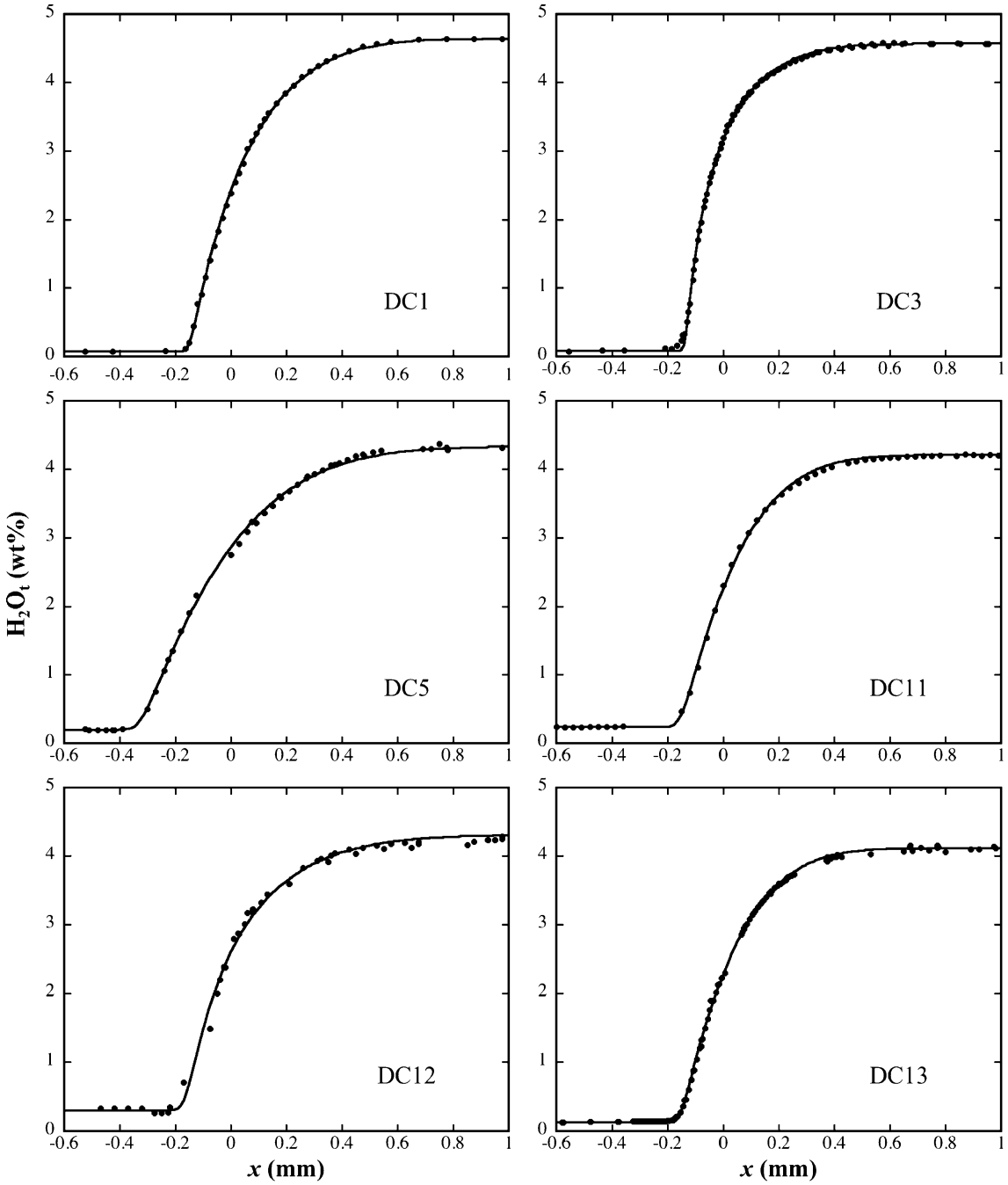


**Fig. 5** Experimental $H_2O_t$ diffusion profiles and fits assuming (1) $D_{OH} \ll D_{H_2O_m}$ and (2) $D_{H_2O_m} = D_0 e^{aX}$ where $X$ is mole fraction of $H_2O_t$, and $D_0$ and $a$ are two fitting parameters. There are additional data outside the $x$ range, which are not shown so that the profiles are shown clearly

Delaney and Karsten 1981; Zhang et al. 1991; Zhang and Behrens 2000; Liu et al. 2004; Ni and Zhang 2008; Zhang and Stolper 1991), and has been modeled successfully before. Below, we will model the $H_2O_t$ concentration profiles using concentration-dependent diffusivity, compare $H_2O_t$ diffusivities in peralkaline rhyolite with those in metaluminous rhyolite, and use the data to model bubble growth in Changbai peralkaline rhyolitic melt.

## Discussion

### Modeling water diffusion

As the diffusion profile near the center cylindrical axis is unaffected by water loss from other boundaries, it is treated as one-dimensional diffusion, and the corresponding diffusion equation for $H_2O_t$ is:

$$\frac{\partial X}{\partial t} = \frac{\partial}{\partial x}\left(D_{H_2O_t}\frac{\partial X}{\partial x}\right), \quad (4)$$

where $X = [H_2O_t]$ is the molar fraction of total water on a single oxygen basis (Stolper 1982; Zhang 1999b), $t$ is time, $x$ is distance, and $D_{H_2O_t}$ is the diffusivity (effective binary diffusivity) of $H_2O_t$. The mole fraction $X$ is calculated as $(C/18.015)/[C/18.015 + (100 - C)/33.14]$, where $C$ is $H_2O_t$ in wt%, 18.015 is the molar mass of water, and 33.14 is the average molar mass of Changbai peralkaline rhyolite and NSL on a single oxygen basis.

The shape of the $H_2O_t$ diffusion profiles in Figs. 4 and 5 indicate $H_2O_t$ diffusivity ($D_{H_2O_t}$) increases with $H_2O_t$ content. Fitting the profiles by an error function (long-dashed curve in Fig. 4), i.e., assuming $D_{H_2O_t}$ is a constant, does not work well. One simple approach is to assume $D_{H_2O_t}$ is proportional to $H_2O_t$ content. This assumption works well when $H_2O_t$ is low, e.g., when $H_2O_t$ <2 wt% for rhyolitic melt (e.g., Behrens and Zhang 2009). Our data covers a greater $H_2O_t$ range. Figure 4 shows that the data at 789 K cannot be fit well by assuming $D_{H_2O_t}$ is proportional to $H_2O_t$ (short dashed curve); therefore, a more general diffusion model is necessary.

Because dissolved $H_2O$ component is present in silicate melts as at least two species (Stolper 1982), $H_2O_m$ and OH, and because the two species are unlikely to diffuse at the same rate, a mechanistic approach to $H_2O$ diffusion is to include diffusive flux of both species as:

$$\frac{\partial X}{\partial t} = \frac{\partial}{\partial x}\left(D_{H_2O_m}\frac{\partial X_m}{\partial x} + \frac{1}{2}D_{OH}\frac{\partial X_{OH}}{\partial x}\right), \quad (5)$$

where $X_m$ is the mole fraction of $H_2O_m$, $X_{OH}$ is the mole fraction of OH, and $D_{H_2O_m}$ and $D_{OH}$ are the diffusivities of $H_2O_m$ and OH. The factor 1/2 is due to the fact that one mole of $H_2O$ reacts to form two moles of OH. Zhang et al. (1991) developed this approach and showed that $D_{OH} \ll D_{H_2O_m}$ in rhyolitic melt so that diffusive flux due to OH diffusion can be ignored. Hence, the above equation can be simplified as:

$$\frac{\partial [H_2O_t]}{\partial t} = \frac{\partial}{\partial x}\left(D_{H_2O_m}\frac{\partial [H_2O_m]}{\partial x}\right). \quad (6)$$

Comparing Eqs. 6 and 4 leads to

$$D_{H_2O_t} = D_{H_2O_m}\left(\frac{\partial X_m}{\partial X}\right)_t, \quad (7)$$

where the subscript $t$ on the derivative means holding $t$ as a constant in this partial derivative. If the temperature is higher than some threshold temperatures (e.g., 800 K, depending on $H_2O_t$), local equilibrium between $H_2O_m$ and OH is reached based on reaction kinetics considerations (e.g., Zhang et al. 1991, 1995; Zhang 1994), i.e., $X_m$ can be determined by just knowing the value of $X$, and the equation above can be written as

$$D_{H_2O_t} = D_{H_2O_m}\frac{dX_m}{dX}. \quad (8)$$

The equilibrium constant of water species reaction, $H_2O_m + O \rightleftharpoons 2OH$, is as follows:

$$K = \frac{[OH]^2}{[H_2O_m][O]}, \quad (9)$$

where the molar fractions are on a single oxygen basis (Stolper 1982). After some steps, the derivative in Eq. 8 can be expressed as:

$$\frac{dX_m}{dX} = 1 - \frac{(0.5 - X)}{\sqrt{X(1-X)(\frac{4}{K} - 1) + 0.25}}, \quad (10)$$

which is a simplified version of Eq. 4 in Zhang and Behrens (2000).

In addition to the assumption that $H_2O_m$ is the diffusing species, we follow Zhang and Behrens (2000) to assume that $D_{H_2O_m}$ in rhyolitic melt depends on $X$ exponentially,

$$D_{H_2O_m} = D_0 e^{aX}. \quad (11)$$

The assumed exponential dependence of the diffusivity of a molecular species on $H_2O_t$ content (or linear dependence of ln $D$ to $X$) in the above equation not only accounts for the $H_2O$ diffusion data well (Zhang and Behrens 2000; Liu et al. 2004; Ni and Zhang 2008; Ni et al. 2009a; this work), but also is supported by experimental data on diffusion of molecular species of $CO_2$ (Watson 1991) and Ar (Behrens and Zhang 2001) in metaluminous rhyolite. Because the IR calibration for the peralkaline rhyolite is not very accurate (meaning species concentrations are not known as well as $H_2O_t$) but $K$ values are nonetheless similar to those for metaluminous rhyolite (Behrens and Zhang 2009), the equilibrium constant $K$ as a function of temperature is not determined experimentally. Instead, we assume that the expression of $K$ in peralkaline rhyolitic melt is the same as that in metaluminous rhyolitic melt (Zhang et al. 1997a):

$$K = e^{1.876 - 3110/T}, \quad (12)$$

where $T$ is the temperature in K. Even though there is uncertainty in $K$, which would affect the model $D_{H_2O_m}$ values, the values of $D_{H_2O_t}$ are largely constrained by the lengths of concentration profiles and hence are not significantly affected by the choice of $K$ values. With these assumptions, every diffusion profile in Figs. 4 and 5 can be fit to obtain two parameters in Eq. 11, $a$ and $D_0$.

The profile fitting program of Ni and Zhang (2008) was used in this study to simultaneously extract $D_0$ and $a$ from

**Table 3** Parameters obtained from fitting the diffusion profiles

| Exp. # | $T$ (K) | $P$ (GPa) | $a$ | $D_0$ (1) ($\mu m^2\ s^{-1}$) | $D_0$ (2) ($\mu m^2\ s^{-1}$) |
|---|---|---|---|---|---|
| CB-PR-DC1 | 1,297 ± 10 | 0.47 | 15.5 ± 1.1 | 31.5 | 28.3 ± 0.8 |
| CB-PR-DC2 | 789 ± 10 | 0.47 | 51.1 ± 1.6 | 0.0209 | 0.0231 ± 0.0008 |
| CB-PR-DC3 | 944 ± 10 | 0.47 | 35.4 ± 1.4 | 0.60 | 0.58 ± 0.01 |
| CB-PR-DC5 | 1,516 ± 15 | 1.42 | 9.1 ± 3.0 | 148 | 131 ± 5 |
| CB-PR-DC11 | 1,506 ± 15 | 0.47 | 17.6 ± 1.8 | 108 | 131 ± 4 |
| CB-PR-DC12 | 951 ± 15 | 0.47 | 29.6 ± 5.5 | 1.1 | 0.9 ± 0.1 |
| CB-PR-DC13 | 1,496 ± 15 | 0.95 | 15.0 ± 1.3 | 70 | 76 ± 1 |
| NSLDC11 | 1,273 | 0.5 | | | 35 ± 1 |
| NSLDC12 | 1,493 | 0.5 | | | 111 ± 9 |
| NSLDC13 | 1,265 | 0.5 | | | 28 ± 2 |
| NSLDC14 | 1,269 | 0.1 | | | 71 ± 5 |
| NSLDC15 | 1,373 | 0.5 | | | 88 ± 10 |
| NSLDC16 | 1,523 | 0.5 | | | 188 ± 13 |
| NSLDC17 | 1,523 | 0.1 | | | 233 ± 22 |
| NSLD12P | 873 | 0.5 | | | 0.21 ± 0.01 |
| NSLD16P | 812 | 0.5 | | | 0.057 ± 0.004 |
| NSLD22P | 902 | 0.5 | | | 0.48 ± 0.07 |
| NSLD23P | 834 | 0.5 | | | 0.065 ± 0.004 |
| NSLD24P | 748 | 0.5 | | | 0.0061 ± 0.0004 |
| NSLD27P | 878 | 0.1 | | | 0.44 ± 0.07 |
| NSLD31P | 745 | 0.1 | | | 0.0132 ± 0.0008 |
| NSLD33P | 771 | 0.5 | | | 0.015 ± 0.002 |

Errors are given at the $2\sigma$ level. CB experimental data are from this study. NSL experimental data are from Behrens and Zhang (2009). $D_0$ (1) is obtained by fitting a given concentration profile to obtain both $a$ and $D_0$ simultaneously. $D_0$ (2) is obtained by fitting the profile when $a$ is fixed to be $a = -27.867 + 60559/T$

each profile. The obtained values of $a$ and their $2\sigma$ error are listed in Table 3.

In Eq. 11, $\ln D_{H_2O_m} = \ln D_0 + aX$. That is, $\ln D_{H_2O_m}$ is linear to $X$. Hence, we may write the Arrhenius relation of molecular water diffusivity as:

$$\begin{aligned}\ln D_{H_2O_m} &= A + \frac{B}{T} + C\frac{P}{T} = (A_1 + A_2X) + \frac{B_1 + B_2X}{T} \\ &\quad + (C_1 + C_2X)\frac{P}{T} \\ &= A_1 + \frac{B_1}{T} + C_1\frac{P}{T} + \left(A_2 + \frac{B_2}{T} + C_2\frac{P}{T}\right)X. \quad (13)\end{aligned}$$

In the above equation, both $a$ and $\ln D_0$ in Eq. 11 are linear to $1/T$ as shown by previous studies (Zhang and Behrens 2000; Ni and Zhang 2008). Ni and Zhang (2008) showed that for metaluminous rhyolite the dependence of parameter $a$ on pressure is within experimental uncertainty of $a$. Figure 6 shows that for peralkaline rhyolite, there is no clear pressure dependence of the parameter $a$. Therefore, we follow Ni and Zhang (2008) and fit $a$ as a function of only $1/T$ using the program of York (1969):

$$a = -27.867 + 60559/T, \quad (14)$$

where $T$ is temperature in K (Fig. 6).

Because the experimental data in this study are limited, and because the composition of the peralkaline rhyolitic melt (NSL, Table 1) in the $H_2O$ study of Behrens and Zhang (2009) with 13 experiments is very similar to that of CB (Table 1), we combine the two data sets to better constrain the dependence of $H_2O$ diffusivity on $T$, $P$ and $H_2O_t$. The experiments by Behrens and Zhang (2009) are at $H_2O_t \leq 2.3$ wt% and hence cannot constrain the $a$ value

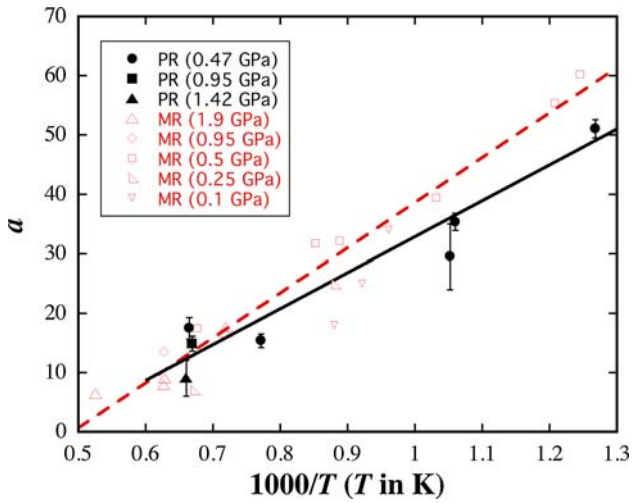


**Fig. 6** The parameter $a$ versus 1,000/$T$. *PR* means peralkaline rhyolite, *MR* means metaluminous rhyolite. The error bars of $a$ are obtained from the fit of the profiles and are shown at the $2\sigma$ level. *Solid symbols and line* are for peralkaline rhyolite (this study) and *open symbols* and the *dashed line* are for metaluminous rhyolite (Ni and Zhang 2008)

well. Hence, we use the $a$ value from Eq. 14 and refit our own data as well as 12 profiles of Behrens and Zhang (2009) to obtain $D_0$ (dehydration profile of NSLD17P in Behrens and Zhang 2009 is excluded in refitting because the profile covers only a very narrow $H_2O_t$ range). The results are listed in Table 3, and shown in Fig. 7. There is good agreement in ln $D_0$ between the CB data to 4.6 wt% $H_2O_t$ and the NSL data to 2.3 wt% $H_2O_t$. Linear regression of ln $D_0$ with respect to $1/T$ and $P/T$ leads to:

$$\ln D_0 = -12.789 - \frac{13939}{T} - 1229.6\frac{P}{T}, \quad (15)$$

where $D_0$ is in $m^2\ s^{-1}$, $T$ is temperature in K and $P$ is pressure in GPa. The maximum deviation from the fit is 0.55 in terms of ln $D_0$. Because there is only one single datum at each of 0.95 and 1.42 GPa, Eq. 15 (as well as Eqs. 16, 17, 18) does not apply well to $P > 0.5$ GPa and is best constrained at $P = 0.5$ GPa.

From Eqs. 11, 14 and 15, $H_2O_m$ diffusivity can be expressed as:

$$D_{H_2O_m} = \exp\left[-12.789 - \frac{13939}{T} - 1229.6\frac{P}{T} + \left(-27.867 + \frac{60559}{T}\right)X\right], \quad (16)$$

where $D_{H_2O_m}$ is in $m^2\ s^{-1}$. Combining Eqs. 8, 10, 12 and 16, $H_2O_t$ diffusivity in peralkaline rhyolite can be calculated from the following equation:

$$D_{H_2O_t} = D_{H_2O_m}\left(1 - \frac{0.5 - X}{\sqrt{[4\exp(3110/T - 1.876) - 1](X - X^2) + 0.25}}\right), \quad (17)$$

where $D_{H_2O_m}$ is from Eq. 16, $T$ is in K, and $X$ is molar fraction of water on a single oxygen basis. The above equation works best at pressures of 0.5 GPa and below.

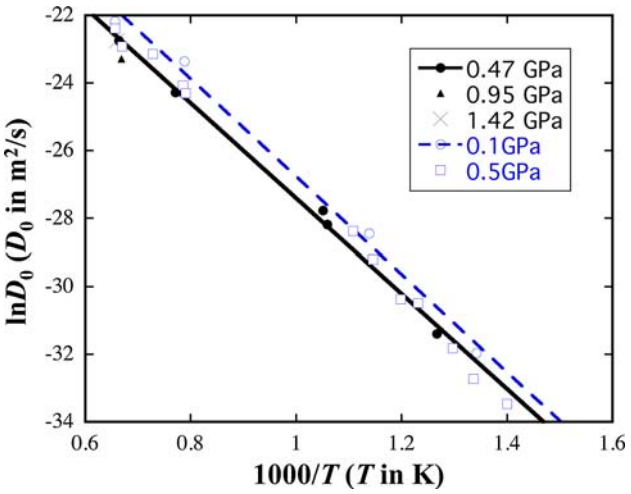


**Fig. 7** ln $D_0$ versus 1,000/$T$. The *open circles and squares* (*in blue*) are data from Behrens and Zhang (2009). The rest are from this study

In the above derivation of the expression for $D_{H_2O_m}$, the equilibrium constant $K$ for metaluminous rhyolite is used for CB. There may be a small systematic error associated with this assumption. For example, if $K$ for peralkaline rhyolite were larger, it would mean less $H_2O_m$ at the same $H_2O_t$, and hence greater $D_{H_2O_m}$ than inferred from this study. So the physical meaning of obtained $D_{H_2O_m}$ might be blurred in this way. However, the $D_{H_2O_t}$ obtained from Eq. 17 is physically meaningful as long as experimental diffusion profiles are well fit.

## Comparison with water diffusivity in metaluminous rhyolite

Since the equilibrium constant (Eq. 9) in peralkaline rhyolite is assumed to be the same as that in metaluminous rhyolite, by comparing the relations for metaluminous rhyolite (Ni and Zhang 2008) and those for peralkaline rhyolite (this work), the relationship between the total water diffusivities in metaluminous and peralkaline rhyolite can be expressed as:

$$D_{H_2O_t(PR)} = D_{H_2O_t(MR)} \times \exp\left(1.47 - 1.89P + 9.39X - \frac{1000 - 2396P + 15325X}{T}\right), \quad (18)$$

where $T$ is in K, $P$ is in GPa, PR stands for peralkaline rhyolite, and MR stands for metaluminous rhyolite. From this expression, in the temperature range of the dataset, i.e., 789–1,516 K, an increase of $X$ would increase $D_{H_2O_t}$ in metaluminous rhyolite more than that in peralkaline rhyolite. Figure 8 illustrates how $D_{H_2O_t}$ in the two melts would vary with $H_2O_t$ and temperature at 0.5 GPa. At 1 wt% $H_2O_t$, $D_{H_2O_t}$ in peralkaline rhyolite is about 1.8 times that in metaluminous rhyolite. At 4.3 wt% $H_2O_t$, the difference is smaller and only becomes noticeable when $T > 1{,}000$ K. The intersection of $H_2O_t$ diffusivities in the two melts at high $H_2O_t$ is due to the larger value of parameter $a$ for $H_2O$ diffusion in metaluminous rhyolite. Contrary to our expectation based on viscosity differences, the boost of water diffusivity in peralkaline rhyolite compared to metaluminous rhyolite is quite limited.

In summary, even though at 1,123 K the viscosity of metaluminous rhyolitic melt is a factor of 10–450 times that of peralkaline rhyolitic melt based on the viscosity model of Hui and Zhang (2007), the difference in $H_2O$ diffusivity is less than a factor of 2. Because another general viscosity model was published more recently (Giordano et al. 2008), there is some concern about which viscosity model is better suited for the prediction of viscosities of metaluminous and peralkaline rhyolites. As shown by Table 3 of Giordano et al. (2008), their viscosity database for F-free compositions

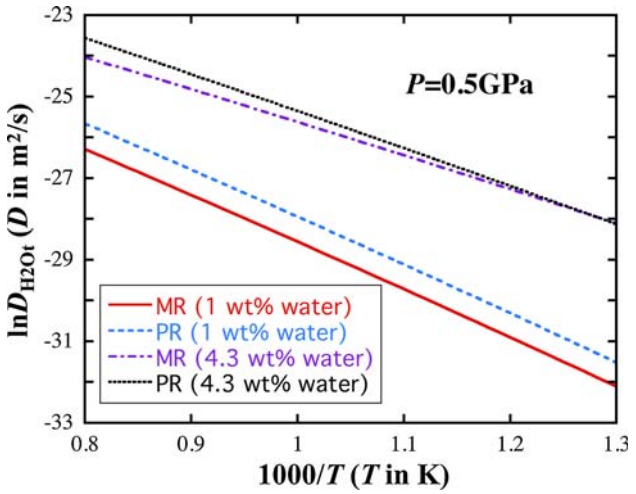


**Fig. 8** Comparison of total water diffusivities in peralkaline rhyolite (PR) and metaluminous rhyolite (MR)

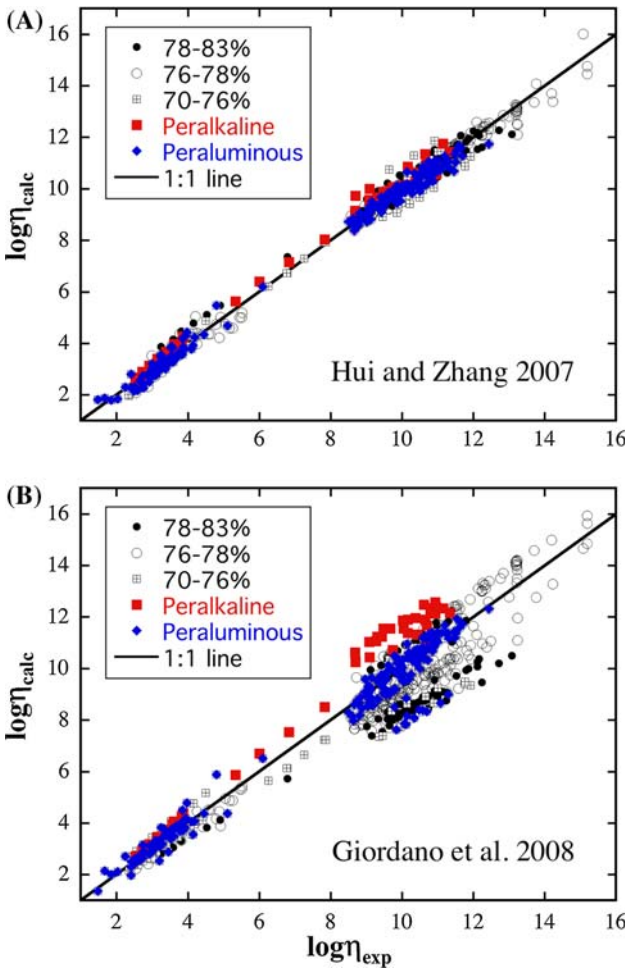


**Fig. 9** Viscosity models of Hui and Zhang (2007) and Giordano et al. (2008) compared to experimental data. The percentages in the legends refer to $SiO_2$ wt%. Data sources: Hess et al. (1995) and Dingwell et al. (1998) for peralkaline rhyolites; see references in Hui and Zhang (2007) for data sources of other rhyolites. Peralkaline rhyolites include those with $Na_2O + K_2O–Al_2O_3$ between 0.01 and 0.05 on dry molar basis, and peraluminous rhyolites include those with $Na_2O + K_2O–Al_2O_3$ between −0.01 and −0.06 on dry molar basis

(1,508 points) can be reproduced to roughly the same precision by the models of Hui and Zhang (2007) and Giordano et al. (2008) (0.53 vs. 0.41 for error in log $\eta$). On the other hand, the viscosity database (1,451 points) used by Hui and Zhang (2007) is much better reproduced by the model of Hui and Zhang (2007) than by the model of Giordano et al. (2008) (0.31 vs. 0.82 for error in log $\eta$). More specifically, we compare the two models for rhyolitic melts in Fig. 9. For peralkaline rhyolite such as CB and NSL, no viscosity data are available for direct comparison. Nonetheless, Hess et al. (1995) and Dingwell et al. (1998) reported viscosity data for synthetic peralkaline rhyolites, some of which are close enough to CB and NSL compositions used in this work. Because $Na_2O + K_2O–Al_2O_3$ (on dry and molar basis) in our peralkaline rhyolite is $\leq$0.023, we restricted the comparison between models and experimental data to silicic melts with $SiO_2$ >70 wt% and $|Na_2O + K_2O–Al_2O_3| \leq 0.06$. In Fig. 9a, experimental data are compared with the model of Hui and Zhang (2007); in Fig. 9b, experimental data are compared with the model of Giordano et al. (2008). As shown by Fig. 9a, b, the model of Hui and Zhang (2007) reproduced the viscosity data of metaluminous, peralkaline and peraluminous rhyolites much better that that of Giordano et al. (2008). Hence, we choose the model of Hui and Zhang (2007) to calculate viscosity of metaluminous and peralkaline rhyolites here as well as later for bubble growth calculation.

The small difference in diffusivity cannot be predicted a priori from viscosity difference or other parameters. The decoupling between $H_2O$ diffusivity and viscosity of metaluminous and peralkaline rhyolites (i.e., the failure of the Stokes–Einstein equation in predicting diffusivities of neutral molecular species in silicate melts) is consistent with previous discussion (e.g., Chen et al. 1982 for diffusion in cyclohexane; Ni and Zhang 2008 for diffusion in a silicate melt). A number of authors have also discussed its inapplicability to diffusion of ionic species in silicate melts (e.g., Magaritz and Hofmann 1978; Chakraborty 1995) but the Stokes–Einstein relation is intended only for neutral particles.

## Bubble growth in Mount Changbai peralkaline rhyolitic melt

Bubble growth is a key process in explosive volcanic eruptions, in which volatile diffusivity, solubility and melt viscosity play critical roles. Below, the program of Proussevitch and Sahagian (1998) modified by Liu and Zhang (2000) is adapted to compare the bubble growth rates in hydrous metaluminous and peralkaline rhyolites at

1,123 K (a typical eruption temperature for rhyolite). The initial $H_2O_t$ in the calculation is taken to be 5.16 wt% (water content in the pre-eruptive peralkaline rhyolitic melt in the ~1,000 AD eruption of Mount Changbai, Horn and Schmincke 2000). The calculation was carried out for confining pressures of 100, 10, 1, and 0.1 MPa. Melt viscosity model is from Hui and Zhang (2007); model of water solubility in silicate melt is from Zhang et al. (2007), which is in good agreement with experimental data of "normal" rhyolite as well as peralkaline rhyolite melt (e.g., Behrens and Jantos 2001). Model of water diffusivity in metaluminous rhyolite is from Ni and Zhang (2008), and that in peralkaline rhyolite is from this study. Although the $H_2O_t$ concentration covered in this study (up to 4.6 wt% $H_2O_t$) is less than 5.16 wt%, because for metaluminous rhyolite $H_2O_t$ in diffusion studies is up to 7.7 wt% and because $D_{H_2O_t}$ in peralkaline rhyolite is only slightly different from that in metaluminous rhyolite, we expect that small extrapolation of our diffusivity expression to 5.16 wt% $H_2O_t$ is acceptable.

Figure 10 shows the calculated results. In our isothermal bubble growth simulation at a constant confining pressure, at high confining pressures (e.g., 100 MPa), the bubble growth curve is roughly parabolic (Fig. 10d), meaning bubble growth is mainly controlled by diffusion. Under such conditions, bubble growth curves for metaluminous and peralkaline rhyolitic melts almost overlap, which is not surprising because water diffusivities are close, especially at high water content. However, as confining pressures decreases (1–10 MPa), viscosity plays a more important role and bubble growth curves for metaluminous and peralkaline rhyolitic melts start to separate from each other (Fig. 10b, c). At even lower confining pressure (e.g., 0.1 MPa), bubbles growing in peralkaline rhyolitic melt follow a much faster exponential curve (Fig. 10a), indicating bubble growth is mainly controlled by viscosity (Lensky et al. 2004). The

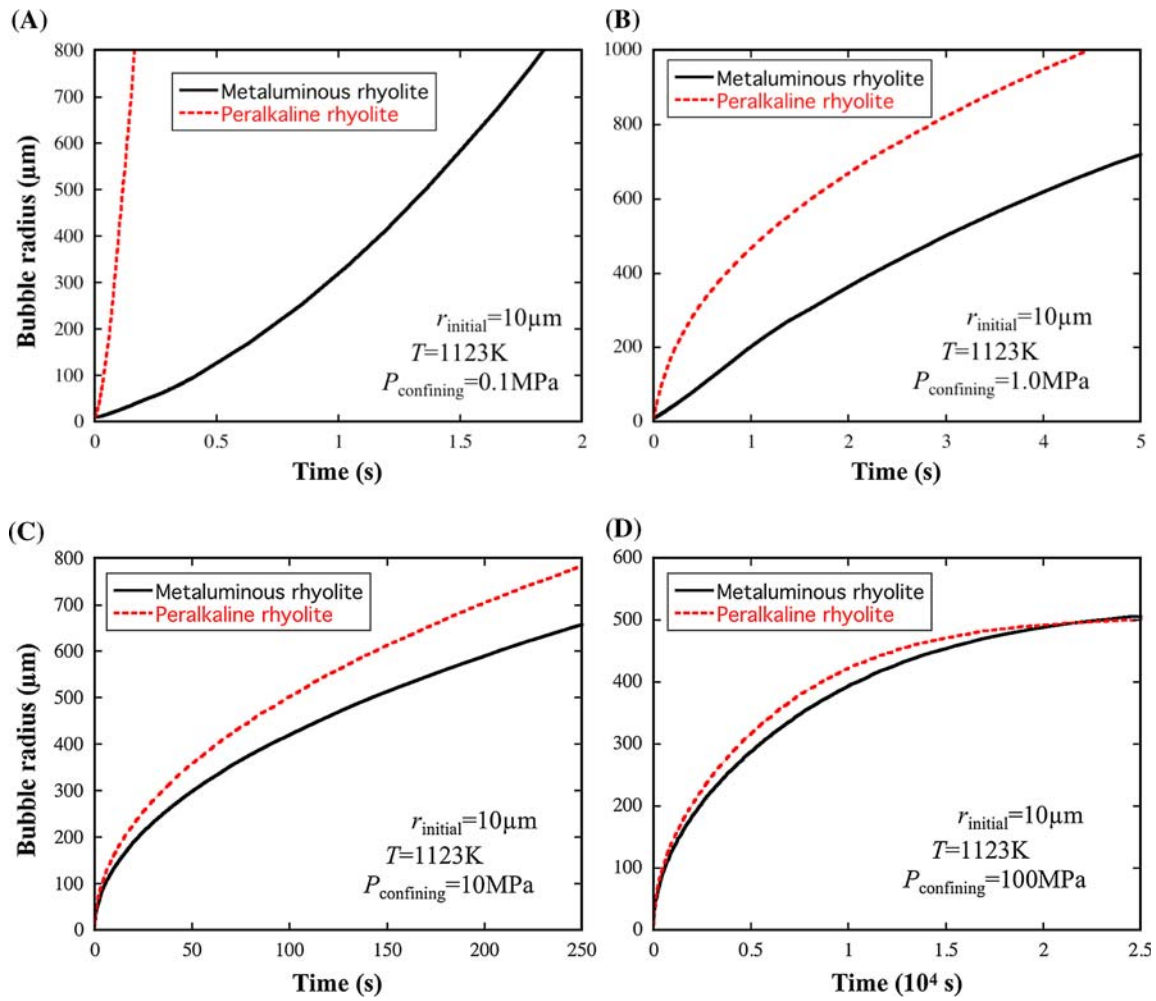


**Fig. 10** Comparison of $H_2O$ bubble growth rate in peralkaline and metaluminous rhyolitic melts. In the calculation, the initial bubble radius is taken to be 10 μm, the initial melt sphere radius is 1000 μm, and the initial $H_2O_t$ in the calculation is taken to be 5.16 wt% (water content in pre-eruptive melt of Mount Changbai Volcano, Horn and Schmincke 2000)

orders of magnitude difference in viscosity between metaluminous and peralkaline rhyolitic melts result in large contrast in bubble growth rates, as seen in Fig. 10a, b. The much greater bubble growth rate in peralkaline rhyolite than in metaluminous rhyolite at low confining pressure (near the conduit exit) may result in more violent eruptions for peralkaline rhyolites if other conditions are equal.

Higher growth rate for both melts at low confining pressure compared to high confining pressure is due to both faster diffusive transport to bubbles (due to larger $H_2O_t$ concentration gradient) and lower density of gas. The control of bubble growth by diffusion at high confining pressure but by viscosity at low confining pressure can be explained as follows. When the confining pressure is high, $H_2O_t$ concentration in the melt is high, leading to low viscosity. Therefore, viscosity does not limit bubble growth rate. On the other hand, when the confining pressure is low, $H_2O_t$ concentration in the melt adjacent to the bubble is low, leading to high viscosity. Hence, viscous bubble expansion becomes the limiting factor.

## Conclusions

Diffusion couple experiments with high water content (up to 4.6 wt%) were carried out to investigate water diffusion in peralkaline rhyolite. Assuming the same equilibrium constant of water species reaction in peralkaline rhyolite as in metaluminous rhyolite, the dependence of $H_2O_m$ and $H_2O_t$ diffusivity on temperature, pressure and water content is obtained. The overall excellence of fitting quality indicates that the method in this study captures the essence of water diffusion. The formulated total water diffusivity (Eq. 17) can be applied at 789–1516 K, 0–0.5 GPa, and 0–4.6 wt% of water. $H_2O_t$ diffusivity in peralkaline rhyolite is within a factor of 2 of that in metaluminous rhyolite, while the corresponding viscosity is small by 1.0–2.6 orders of magnitude. Hence, the Stokes–Einstein equation relating diffusivity of neutral species and viscosity does not apply here. Preliminary bubble growth calculation shows that for a melt containing 5.16 wt% water, at high confining pressures, bubble growth is limited by diffusivity, leading to small difference in bubble growth rates in metaluminous and peralkaline rhyolitic melts. On the other hand, at low confining pressures viscosity plays a more important role and hence growth rate in peralkaline rhyolitic melt is much greater than that in metaluminous rhyolitic melts. In explosive volcanic eruptions, the confining pressure on the melt varies with magma ascent and the two stages (diffusion control vs. viscosity control) are intertwined. Hence, the difference in volcanic eruption dynamics between peralkaline and metaluminous rhyolites needs further investigation using eruption models.

**Acknowledgments** We thank Bruce Watson and an anonymous reviewer for their insightful and constructive comments, and Huaiwei Ni for providing a sketch of the experimental assembly. H.W. thanks Huaiwei Ni for both helps in the lab and constructive discussion about water diffusion. This research is supported by Chinese NSF grant 40640420141 and US NSF grant EAR-0537598 and EAR-0711050.

## References

Behrens H, Jantos N (2001) The effect of anhydrous composition on water solubility in granitic melts. Am Mineral 86:14–20

Behrens H, Nowak M (2003) Quantification of $H_2O$ speciation in silicate glasses and melts by IR spectroscopy—in situ versus quench techniques. Phase Transit 76:45–61. doi:10.1080/01411590310000076048

Behrens H, Zhang Y (2001) Ar diffusion in hydrous silicic melts: implications for volatile diffusion mechanisms and fractionation. Earth Planet Sci Lett 192:363–376. doi:10.1016/S0012-821X(01)00458-7

Behrens H, Zhang Y (2009) $H_2O$ diffusion in peralkaline to peraluminous rhyolitic melts. Contrib Mineral Petrol 157. doi:10.1007/s00410-00008-00363-00414

Behrens H, Romano C, Nowak M, Holtz F, Dingwell DB (1996) Near-infrared spectroscopic determination of water species in glasses of the system $MAlSi_3O_8$ (M = Li, Na, K): an interlaboratory study. Chem Geol 128:41–63. doi:10.1016/0009-2541(95)00162-X

Behrens H, Zhang Y, Xu Z (2004) $H_2O$ diffusion in dacitic and andesitic melts. Geochim Cosmochim Acta 68:5139–5150. doi:10.1016/j.gca.2004.07.008

Blower JD, Mader HM, Wilson SDR (2001) Coupling of viscous and diffusive controls on bubble growth during explosive volcanic eruptions. Earth Planet Sci Lett 193:47–56. doi:10.1016/S0012-821X(01)00488-5

Chakraborty S (1995) Diffusion in silicate melts. Rev Mineral 32:411–503

Chen SH, Davis HT, Evans DF (1982) Tracer diffusion in polyatomic liquids. II. J Chem Phys 75:1422–1426. doi:10.1063/1.442148

Delaney JR, Karsten JL (1981) Ion microprobe studies of water in silicate melts: concentration-dependent water diffusion in obsidian. Earth Planet Sci Lett 52:191–202. doi:10.1016/0012-821X(81)90220-X

Dingwell DB, Hess KU, Romano C (1998) Extremely fluid behavior of hydrous peralkaline rhyolites. Earth Planet Sci Lett 158:31–38. doi:10.1016/S0012-821X(98)00046-6

Einstein A (1905) The motion of small particles suspended in static liquids required by the molecular kinetic theory of heat. Ann Phys 17:549–560. doi:10.1002/andp.19053220806 (in German)

Ganguly J, Bhattacharya RN, Chakraborty S (1988) Convolution effect in the determination of compositional profiles and diffusion coefficients by microprobe step scans. Am Mineral 73:901–909

Giordano D, Russell JK, Dingwell DB (2008) Viscosity of magmatic liquids: a model. Earth Planet Sci Lett 271:123–134. doi:10.1016/j.epsl.2008.03.038

Hess KU, Dingwell DB, Webb SL (1995) The influence of excess alkalies on the viscosity of a haplogranitic melt. Am Mineral 80:297–304

Horn S, Schmincke HU (2000) Volatile emission during the eruption of Baitoushan Volcano (China/North Korea) ca. 969 AD. Bull Volcanol 61:537–555

Hui H, Zhang Y (2007) Toward a general viscosity equation for natural anhydrous and hydrous silicate melts. Geochim Cosmochim Acta 71:403–416. doi:10.1016/j.gca.2006.09.003

Hui H, Zhang Y, Xu Z, Behrens H (2008) Pressure dependence of the speciation of dissolved water in rhyolitic melts. Geochim Cosmochim Acta 72:3229–3240. doi:10.1016/j.gca.2008.03.025

Jin B, Zhang X (1994) Volcanic geology of Mount Changbai (in Chinese). Dongbei Korean Ethnic Education Press, p 223

Lensky NG, Navon O, Lyakhovsky V (2004) Bubble growth during decompression of magma: experimental and theoretical investigations. J Volcanol Geotherm Res 129:7–22. doi:10.1016/S0377-0273(03)00229-4

Leschik M, Heide G, Frischat GH, Behrens H, Wiedenbeck M, Wagner N, Heide K, Geissler H, Reinholz U (2004) Determination of $H_2O$ and $D_2O$ contents in rhyolitic glasses using KFT, NRA, EGA, IR spectroscopy, and SIMS. Phys Chem Glasses 45:238–251

Liu Y, Zhang Y (2000) Bubble growth in rhyolitic melt. Earth Planet Sci Lett 181:251–264. doi:10.1016/S0012-821X(00)00197-7

Liu Y, Zhang Y, Behrens H (2004) $H_2O$ diffusion in dacitic melt. Chem Geol 209:327–340. doi:10.1016/j.chemgeo.2004.06.019

Magaritz M, Hofmann AW (1978) Diffusion of Sr, Ba and Na in obsidian. Geochim Cosmochim Acta 42:595–605. doi:10.1016/0016-7037(78)90004-2

Melnik O, Sparks RSJ (1999) Nonlinear dynamics of lava dome extrusion. Nature 402:37–41. doi:10.1038/46950

Moulson AJ, Roberts JP (1961) Water in silica glass. Trans Faraday Soc 57:1208–1216. doi:10.1039/tf9615701208

Newman S, Stolper EM, Epstein S (1986) Measurement of water in rhyolitic glasses: calibration of an infrared spectroscopic technique. Am Mineral 71:1527–1541

Ni H, Zhang Y (2008) $H_2O$ diffusion models in rhyolitic melt with new high pressure data. Chem Geol 250:68–78. doi:10.1016/j.chemgeo.2008.02.011

Ni H, Behrens H, Zhang Y (2009a) A general expression for water diffusivity in dacite melt. Geochim Cosmochim Acta (in revision)

Ni H, Liu Y, Wang L, Zhang Y (2009b) Water speciation and diffusion in haploandesite at 743–873 K and 0.1 GPa. Geochim Cosmochim Acta (in revision)

Nowak M, Behrens H (1997) An experimental investigation on diffusion of water in haplogranitic melts. Contrib Mineral Petrol 126:365–376. doi:10.1007/s004100050256

Ochs FA, Lange RA (1999) The density of hydrous magmatic liquids. Science 283:1314–1317. doi:10.1126/science.283.5406.1314

Ohlhorst S, Behrens H, Holtz F (2001) Compositional dependence of molar absorptivities of near-infrared OH- and $H_2O$ bands in rhyolitic to basaltic glasses. Chem Geol 174:5–20. doi:10.1016/S0009-2541(00)00303-X

Okumura S, Nakashima S (2006) Water diffusion in basaltic to dacitic glasses. Chem Geol 227:70–82. doi:10.1016/j.chemgeo.2005.09.009

Proussevitch AA, Sahagian DL (1998) Dynamics and energetics of bubble growth in magmas: analytical formulation and numerical modeling. J Geophys Res 103:18223–18251. doi:10.1029/98JB00906

Richet P, Whittington A, Holtz F, Behrens H, Ohlhorst S, Wilke M (2000) Water and the density of silicate glasses. Contrib Mineral Petrol 138:337–347. doi:10.1007/s004100050567

Scholze H, Mulfinger HO (1959) Der Einbau des Wassers in Glasern. V. Die Diffusion des Wassers in Glåsern bei hohen Temperaturen. Glastech Ber 32:381–385 (in German)

Self S, Blake S, Sharma K, Widdowson M, Sephton S (2008) Sulfur and chlorine in late Cretaceous Deccan magmas and eruptive gas release. Science 319:1654–1657. doi:10.1126/science.1152830

Shaw HR (1972) Viscosities of magmatic silicate liquids: an empirical method of prediction. Am J Sci 272:870–893

Shaw HR (1974) Diffusion of $H_2O$ in granitic liquids, I: experimental data; II: mass transfer in magma chambers. In: Hofmann AW, Giletti BJ, Yoder HS, Yund RA (eds) Geochemical transport and kinetics, vol 634. Carnegie Institution of Washington, Washington, DC, pp 139–170

Spieler O, Kennedy B, Kueppers U, Dingwell DB, Scheu B, Taddeucci J (2004) The fragmentation threshold of pyroclastic rocks. Earth Planet Sci Lett 226:139–148. doi:10.1016/j.epsl.2004.07.016

Stolper EM (1982) The speciation of water in silicate melts. Geochim Cosmochim Acta 46:2609–2620. doi:10.1016/0016-7037(82)90381-7

Watson EB (1991) Diffusion of dissolved $CO_2$ and Cl in hydrous silicic to intermediate magmas. Geochim Cosmochim Acta 55:1897–1902. doi:10.1016/0016-7037(91)90031-Y

Withers AC, Behrens H (1999) Temperature-induced changes in the NIR spectra of hydrous albitic and rhyolitic glasses between 300 and 100 K. Phys Chem Miner 27:119–132. doi:10.1007/s002690050248

York D (1969) Least-squares fitting of a straight line with correlated errors. Earth Planet Sci Lett 5:320–324. doi:10.1016/S0012-821X(68)80059-7

Zhang Y (1994) Reaction kinetics, geospeedometry, and relaxation theory. Earth Planet Sci Lett 122:373–391. doi:10.1016/0012-821X(94)90009-4

Zhang Y (1999a) A criterion for the fragmentation of bubbly magma based on brittle failure theory. Nature 402:648–650. doi:10.1038/45210

Zhang Y (1999b) $H_2O$ in rhyolitic glasses and melts: measurement, speciation, solubility, and diffusion. Rev Geophys 37:493–516. doi:10.1029/1999RG900012

Zhang Y, Behrens H (2000) H2O diffusion in rhyolitic melts and glasses. Chem Geol 169:243–262. doi:10.1016/S0009-2541(99)00231-4

Zhang Y, Stolper EM (1991) Water diffusion in basaltic melts. Nature 351:306–309. doi:10.1038/351306a0

Zhang Y, Stolper EM, Wasserburg GJ (1991) Diffusion of water in rhyolitic glasses. Geochim Cosmochim Acta 55:441–456. doi:10.1016/0016-7037(91)90003-N

Zhang Y, Stolper EM, Ihinger PD (1995) Kinetics of reaction $H_2O + O = 2OH$ in rhyolitic glasses: preliminary results. Am Mineral 80:593–612

Zhang Y, Belcher R, Ihinger PD, Wang L, Xu Z, Newman S (1997a) New calibration of infrared measurement of water in rhyolitic glasses. Geochim Cosmochim Acta 61:3089–3100. doi:10.1016/S0016-7037(97)00151-8

Zhang Y, Jenkins J, Xu Z (1997b) Kinetics of the reaction $H_2O + O = 2OH$ in rhyolitic glasses upon cooling: geospeedometry and comparison with glass transition. Geochim Cosmochim Acta 61:2167–2173. doi:10.1016/S0016-7037(97)00054-9

Zhang Y, Xu Z, Liu Y (2003) Viscosity of hydrous rhyolitic melts inferred from kinetic experiments, and a new viscosity model. Am Mineral 88:1741–1752

Zhang Y, Xu Z, Zhu M, Wang H (2007) Silicate melt properties and volcanic eruptions. Rev Geophys 45:RG4004. doi:4010.1029/2006RG000216